Supporting Information

Enhancing the graphitization ability of corn-cob-derived lignin by coupling stabilization and hot-pressing

Xiuxia Zhang[a], Xiao Han[a], Jing Liu[b], Fangxiao Feng[a], Chen Liang[c], Linghong Yin[a,], Wangda Qu[a,]**

a. Laboratory of Lignin-based Materials, College of Life Sciences, Qingdao Agricultural University, Qingdao 266109, China.

b. College of New Materials and New Energies, Shenzhen Technology University, Shenzhen, 518116, China.

c. College of Chemistry and Pharmaceutical Sciences, Qingdao Agricultural University, Qingdao 266109, China.

**Corresponding author: Wangda Qu, E-mail: wqu@qau.edu.cn; Linghong Yin, E-mail: lhyin@qau.edu.cn.*

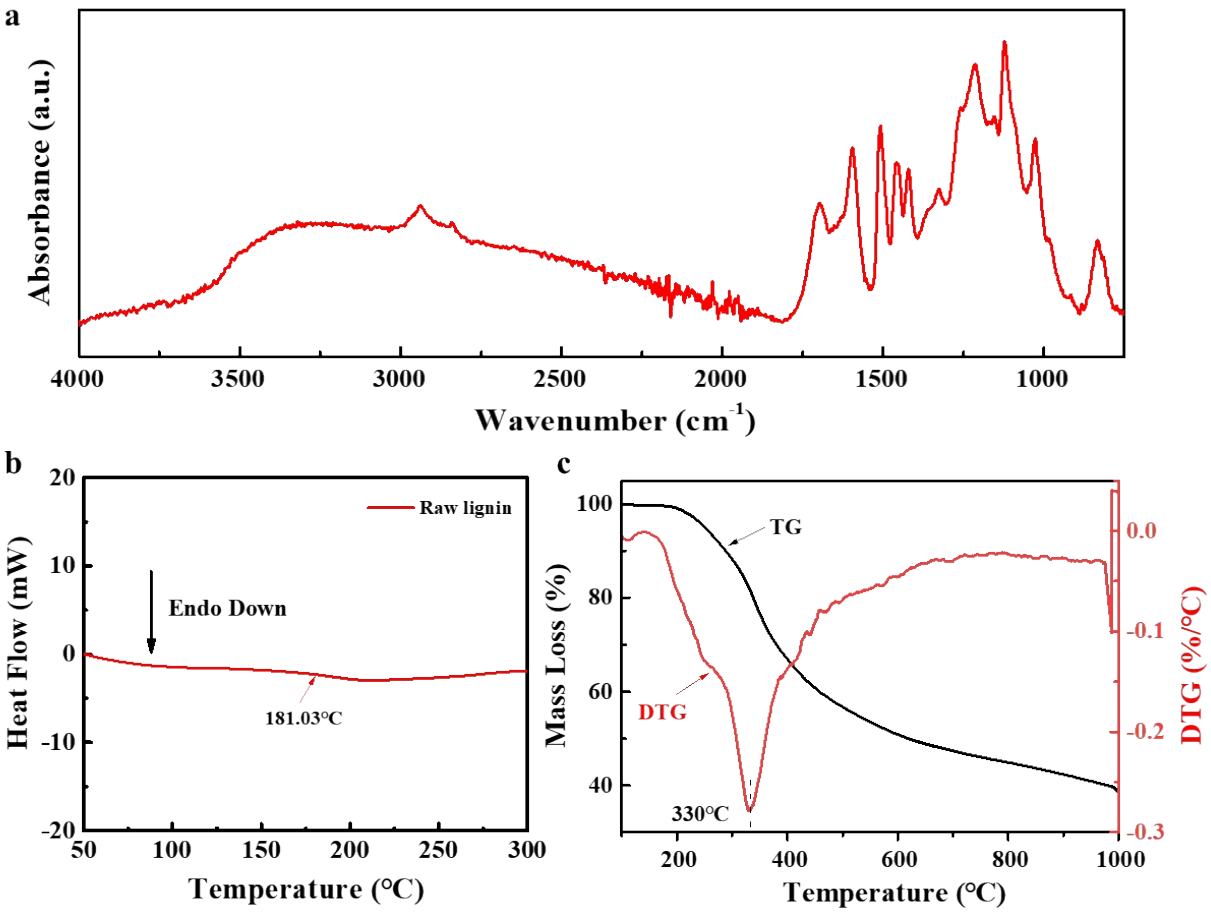

Fig. S1 Characterization of raw lignin: (a) FT-IR spectra; (b) DSC curve; (c) TGA-DTG curves.

Table S1 Peak assignment and distribution of infrared spectra of lignin.

Label	Wavenumbers (cm^{-1})	Assignments
1	2922	C–H stretching of $–OCH_3$ and side chains in lignin
2	2839	C–H stretching of $–OCH_3$ and side chains in lignin
3	1700	C=O stretch in unconjugated ketones, carbonyl ester groups
4	1600	C=O stretching conjugated to the aromatic ring
5	1510	Aromatic ring vibrations
6	1453	C-H in Aromatic rings
7	1421	Aromatic ring vibrations combined with C-H in plane deformation
8	1214	C-C plus C-O plus C=O stretching
9	1116	C-H in plane deformations of syringyl units
10	1029	Aromatic C-H deformation plus C-O deformation in primary alcohols
11	832	C-H vibrations of syringyl units

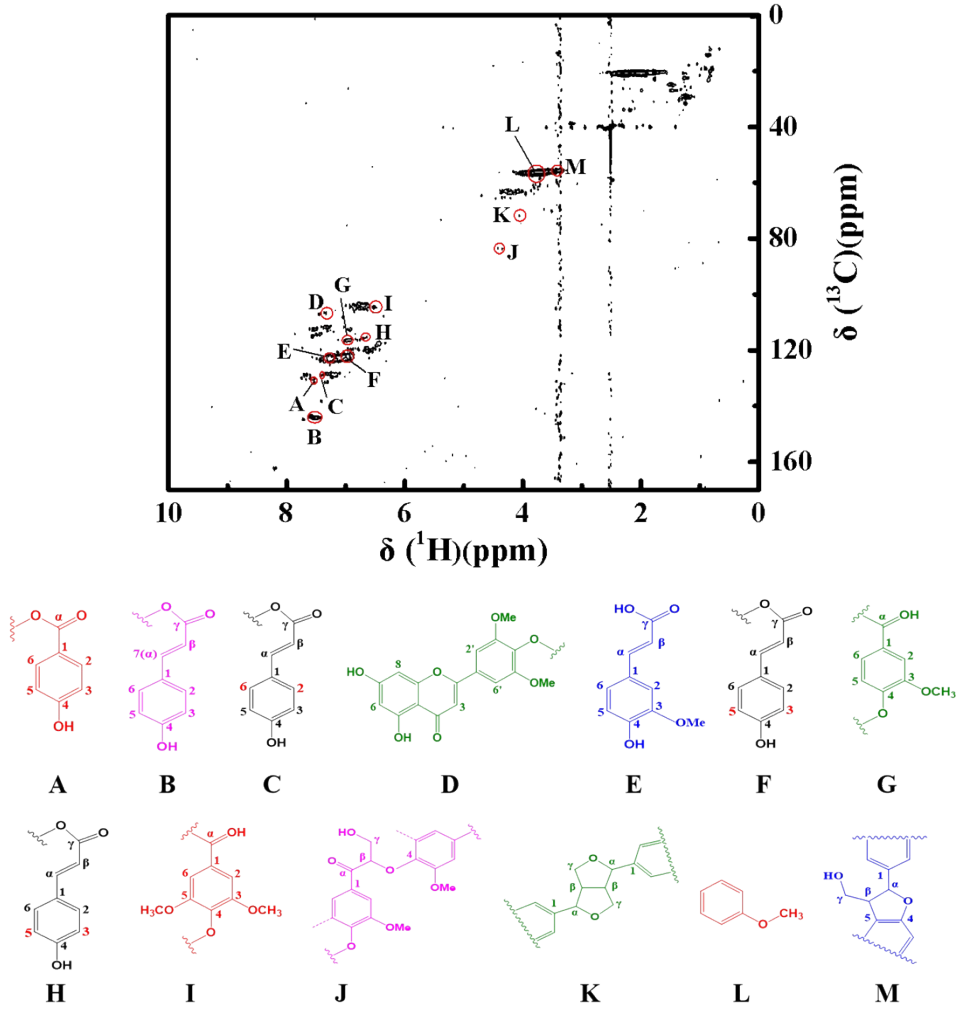

Fig. S2 ^{13}C-^{1}H 2D-HSQC NMR cross-peak spectrum and structural characteristics of A-O linkage in raw lignin.

Table S2 Peak assignment of cross-peaks in ^{13}C-^{1}H 2D-HSQC NMR spectrum of acetylated lignin.

Label	Chemical shift δC/δH (ppm)	Peak assignments
A	131.2/7.67	$C_{2,6}$-$H_{2,6}$ in p-hydroxybenzoate
B	144.8/7.51	C_7–H_7 in p-coumarate
C	130.3/7.48	$C_{2,6}$–$H_{2,6}$ in p-coumarate
D	104.2/7.30	$C_{2,6}$–$H_{2,6}$ in tricin
E	122.5/7.15	C_6–H_6 in ferulate
F	122.0/7.08	$C_{3,5}$–$H_{3,5}$ in p-coumarate
G	116.0/6.95	C_5–H_5 in guaiacyl units
H	115.5/6.79	$C_{3,5}$–$H_{3,5}$ in p-coumarate
I	104.2/6.59	$C_{2,6}$–$H_{2,6}$ in syringyl units
J	83.9/4.29	C_β–H_β in β-O-4
K	71.7/4.06	C_γ-H_γ in β-β resinol
L	56.4/3.77	C–H in methoxyls
M	55.3/3.46	C_β–H_β in phenylcoumarane

Table S3. Residual carbon contents of lignin samples.

Sample	Residual carbon (%)
Raw	38.58
LS-200	39.67
LS-240	43.30
LS-280	47.29
LS-320	53.57
LS-360	60.55
LH-Raw-250-0	44.28
LSH-200-250-15	50.31
LSH-240-250-15	51.97
LSH-280-250-15	54.72
LSH-320-250-15	58.23
LSH-360-250-15	61.28

Table S4. Proportions of different carbon species in lignin samples at different stabilization temperatures via XPS analysis.

Samples	C (%)	O (%)	C-C (%)	C–O (%)	C(O)O (%)
Raw	73.81	26.19	51.78	37.47	10.75
LS-200	70.89	29.11	52.04	40.19	7.77
LS-240	72.91	27.09	52.70	39.22	8.08
LS-280	75.04	24.95	54.34	36.70	8.96
LS-320	75.65	24.35	57.27	32.09	10.64
LS-360	78.91	21.09	60.41	27.61	11.98

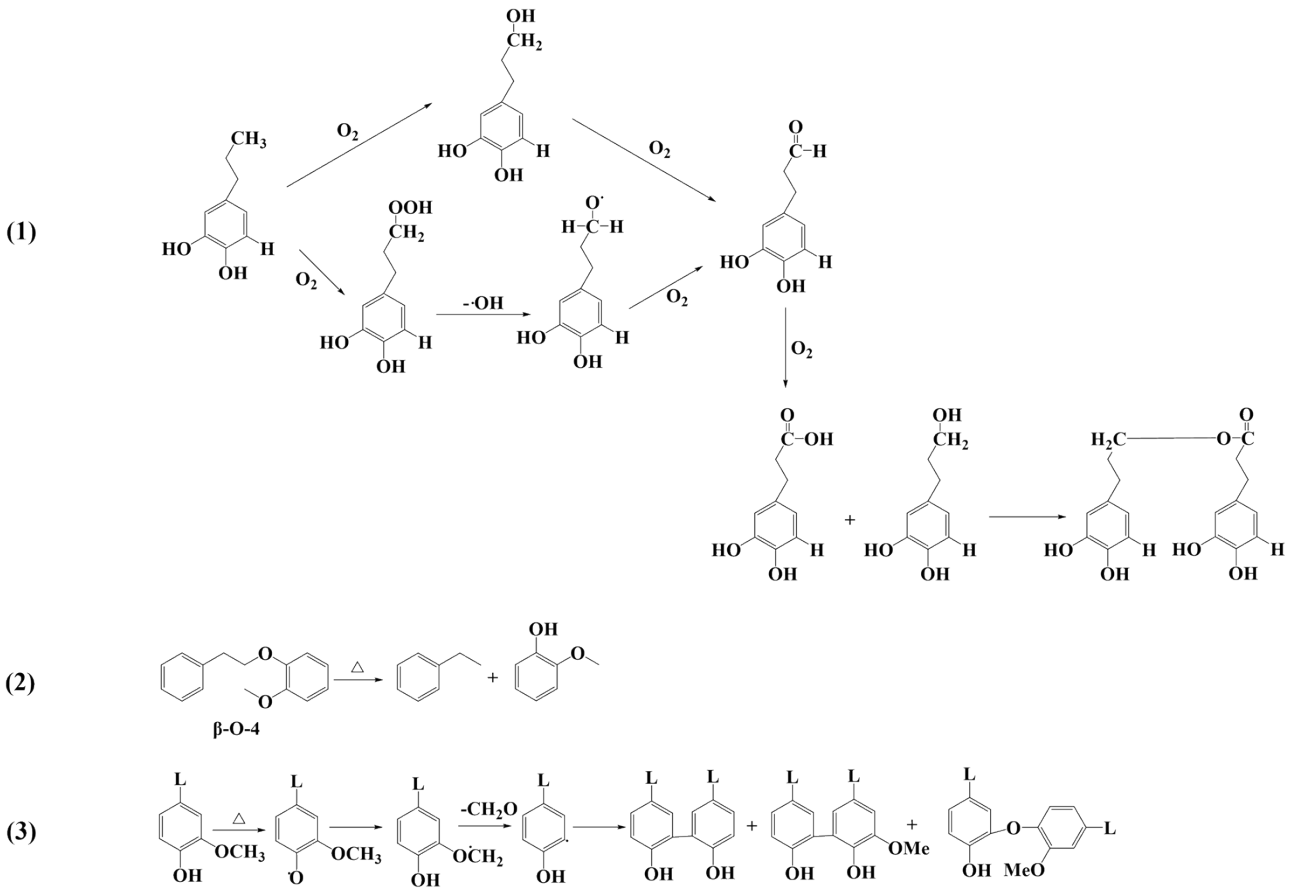

Fig. S3 Stabilization reaction mechanism of lignin during thermal stabilization.[S1-S4]

Table S5 Thickness loss rate of lignin-derived carbon before and after hot-pressing at different stabilization temperatures[a].

Stabilization temperature (℃)	Hot-pressing temperature (℃)	Pressures of hot-pressing (t)	Initial Thickness[b] (mm)	Final thickness[b] (mm)	Thickness loss (%)
Raw	250	0	1.97	6.64	-237.31±2.70
Raw	250	15	1.97	N/A[c]	N/A
200	250	15	1.84	N/A[c]	N/A
240	250	15	1.90	N/A[c]	N/A
280	250	15	1.90	1.05	44.74±0.49
320	250	15	1.92	1.15	40.10±0.45
360	250	15	1.90	N/A[d]	N/A

[a]The thickness measured before and after hot-pressing is the combined thickness of the mold and sample.

[b]The reported value represents the mean of three independent measurements conducted at the central region of the specimen.

[c]After the hot-pressing process, the specimen is ejected from the mold.

[d]Following the hot-pressing process, the specimen maintained its powdered state, rendering it unsuitable for subsequent measurements.

Table S6. Hot-pressing yield, carbonization yield, and overall yield of lignin-derived carbon under different stabilization temperatures.

Stabilization temperature (℃)	Stabilization yield (%)	Hot-pressing yield (%)	Carbonization yield (%)	Overall yield (%)
LHC-Raw-250-0	N/A	80.74	33.04	26.68
LSHC-200-250-15	96.10	N/A	44.92	N/A
LSHC-240-250-15	90.19	N/A	48.99	N/A
LSHC-280-250-15	83.52	90.19	49.68	37.42
LSHC-320-250-15	77.45	92.19	59.16	42.23
LSHC-360-250-15	66.05	N/A[a]	59.11	N/A

[a]The yield at 360 °C hot-pressing is not displayed due to the excessive stabilization temperature, which leads to sufficient cross-linking and the material remaining as powder after hot-pressing. The powder overflows from the mold, causing errors.

Table S7. Lattice parameter comparison of lignin-derived carbon after hot-Pressing at different stabilization temperatures.

Sample	2θ (002) (°)	d_{002}(nm)	FWHM (002) (°)	L_c (nm)
LHC-Raw-250-0	23.55°	0.3778	6.78	1.20
LSHC-200-250-15	23.12°	0.3847	7.17	1.13
LSHC-240-250-15	23.30°	0.3817	6.49	1.25
LSHC-280-250-15	24.44°	0.3641	5.29	1.54
LSHC-320-250-15	24.55°	0.3626	6.09	1.34
LSHC-360-250-15	23.49°	0.3788	5.82	1.39

Table S8 I_D/I_G values of lignin-derived carbon at different stabilization temperatures.

Sample	I_D/I_G
LHC-Raw-250-0	2.85
LSHC-200-250-15	2.62
LSHC-240-250-15	2.36
LSHC-280-250-15	2.31
LSHC-320-250-15	2.17
LSHC-360-250-15	2.61

Table S9. Hot-pressing yield, carbonization yield, and overall yield of lignin-derived carbon under different hot-pressing conditions.

Hot-pressing temperature (℃)	Pressures of hot-pressing (t)	Stabilization yield (℃)	Hot-pressing yield (%)	Carbonization yield (%)	Overall yield (%)
230	15	77.45	91.89	58.22	41.43
250	15	77.45	89.90	58.34	40.62
270	15	77.45	89.76	61.83	42.98
290	15	77.45	87.83	62.81	42.73
230	18	77.45	90.46	53.31	37.35
250	18	77.45	89.97	58.65	40.87
270	18	77.45	89.38	59.05	40.88
290	18	77.45	88.31	61.59	42.13
230	21	77.45	91.58	55.14	39.11
250	21	77.45	90.56	60.32	42.31
270	21	77.45	88.86	61.05	54.25
290	21	77.45	84.08	64.17	42.13

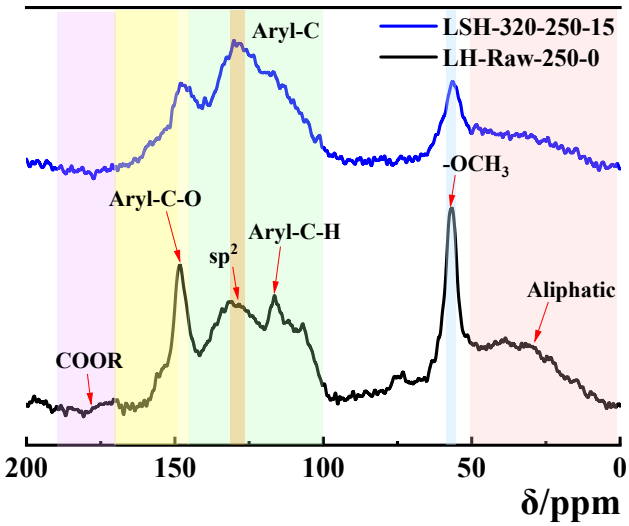

Fig. S4 Solid-state ^{13}C NMR spectra of LH-Raw-250-0 and LSH-320-250-15.

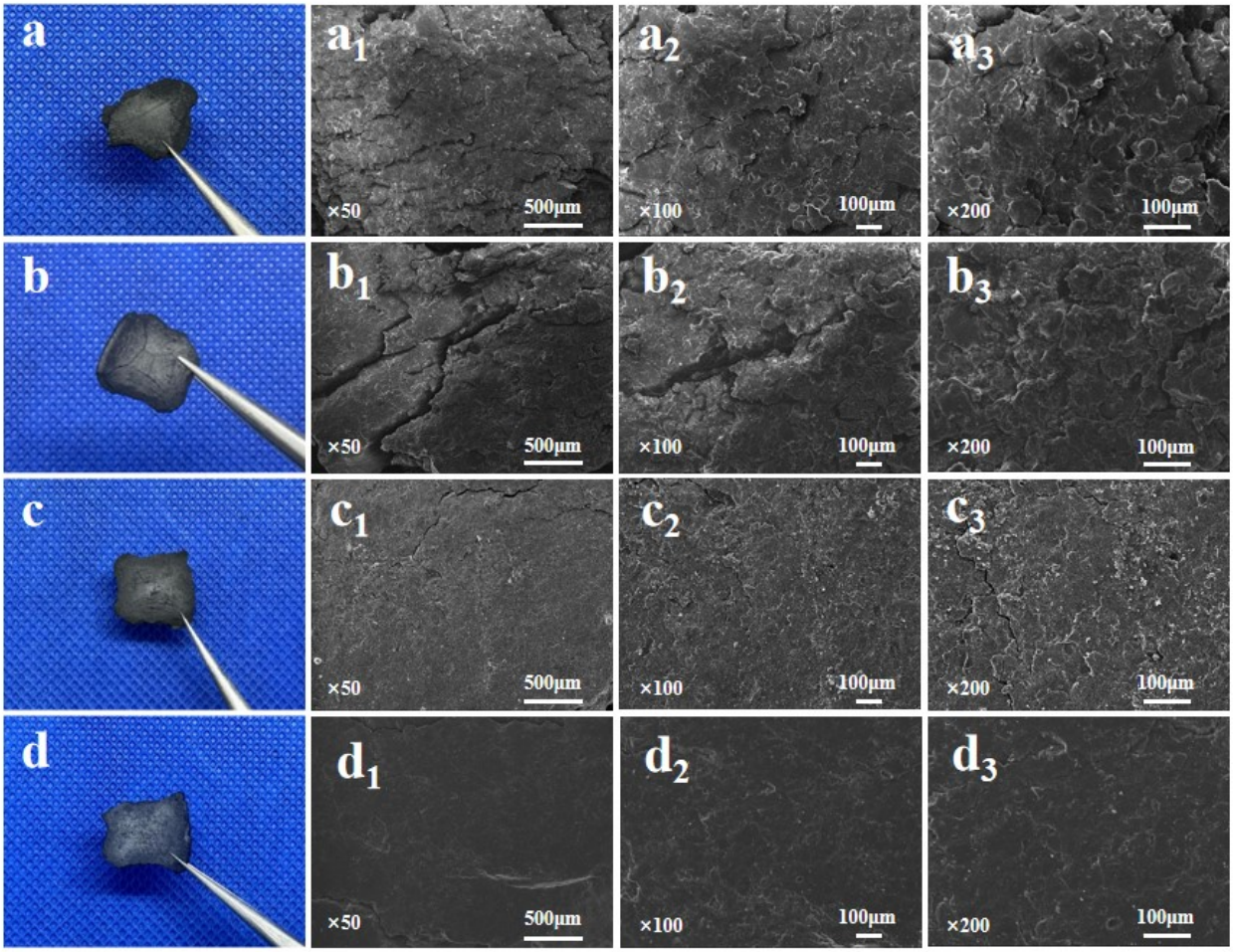

Fig. S5. Morphology and SEM images of LS-320 after hot-pressing under different hot-pressing temperatures: (a) LSH-320-230-15; (b) LSH-320-250-15; (c) LSH-320-270-15; (d) LSH-320-290-15.

Table S10. Thickness loss rate of lignin-derived carbon before and after different hot-pressing conditions[a].

Stabilization temperature (℃)	Hot-pressing temperature (℃)	Pressures of hot-pressing (t)	Initial thickness[b] (mm)	Final thickness[b] (mm)	Thickness Loss (%)
320	230	15	1.78	1.19	33.15±0.34
320	250	15	2.00	1.23	38.50±0.44
320	270	15	1.82	1.11	39.01±0.41
320	290	15	1.80	1.03	42.78±0.44
320	230	18	1.79	1.13	36.87±0.38
320	250	18	1.92	1.15	40.10±0.45
320	270	18	1.99	1.13	43.22±0.50
320	290	18	1.90	1.17	43.68±0.48
320	230	21	1.78	1.10	38.20±0.40
320	250	21	2.04	1.10	46.08±0.53
320	270	21	1.94	1.00	48.45±0.53
320	290	21	1.87	0.93	50.27±0.53

[a]The thickness measured before and after hot-pressing is the combined thickness of the mold and sample.

[b]The reported value represents the mean of three independent measurements conducted at the central region of the specimen.

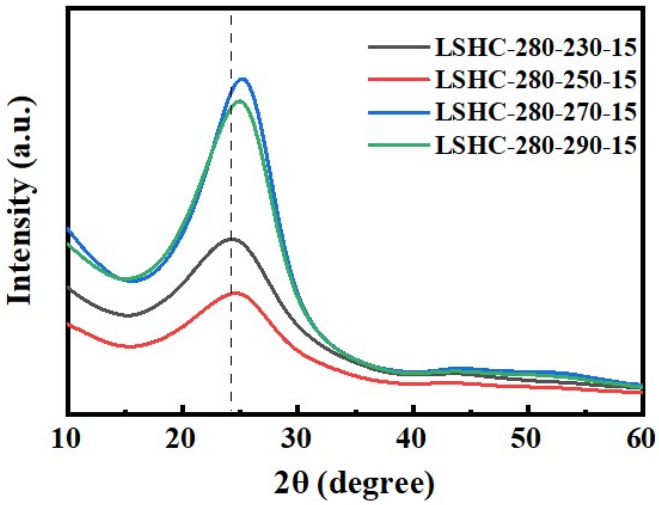

Fig. S6. X-ray diffraction profiles of LSHC-280-230-15, LSHC-280-250-15, LSHC-280-270-15, LSHC-280-290-15.

Table S11. Lattice parameter comparison of lignin-derived carbons stabilized at 280°C under different hot-pressing temperatures.

Sample	2θ (002) (°)	d_{002} (nm)	FWHM (002) (°)	L_c (nm)
LSHC-280-230-15	24.30	0.3662	6.30	1.29
LSHC-280-250-15	24.44	0.3641	5.29	1.54
LSHC-280-270-15	24.78	0.3456	5.29	1.54
LSHC-280-290-15	24.50	0.3633	5.61	1.45

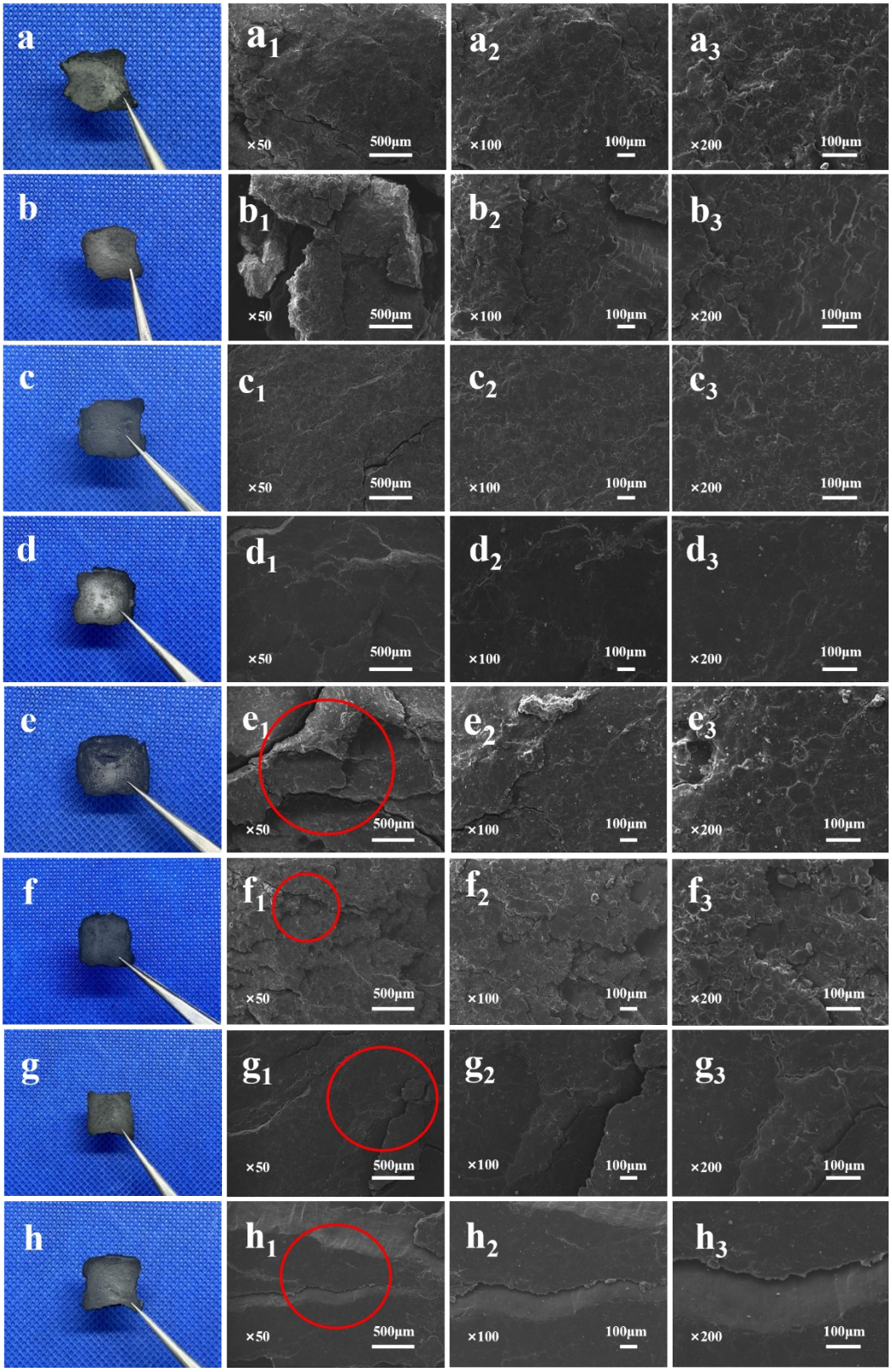

Fig. S7. Morphology and SEM images of LS-320 after hot-pressing under different hot-pressing conditions: (a) LSH-320-230-18; (b) LSH-320-250-18; (c) LSH-320-270-18; (d) LSH-320-290-18; (e) LSH-320-230-21; (f) LSH-320-250-21; (g) LSH-320-270-21; (h) LSH-320-290-21.

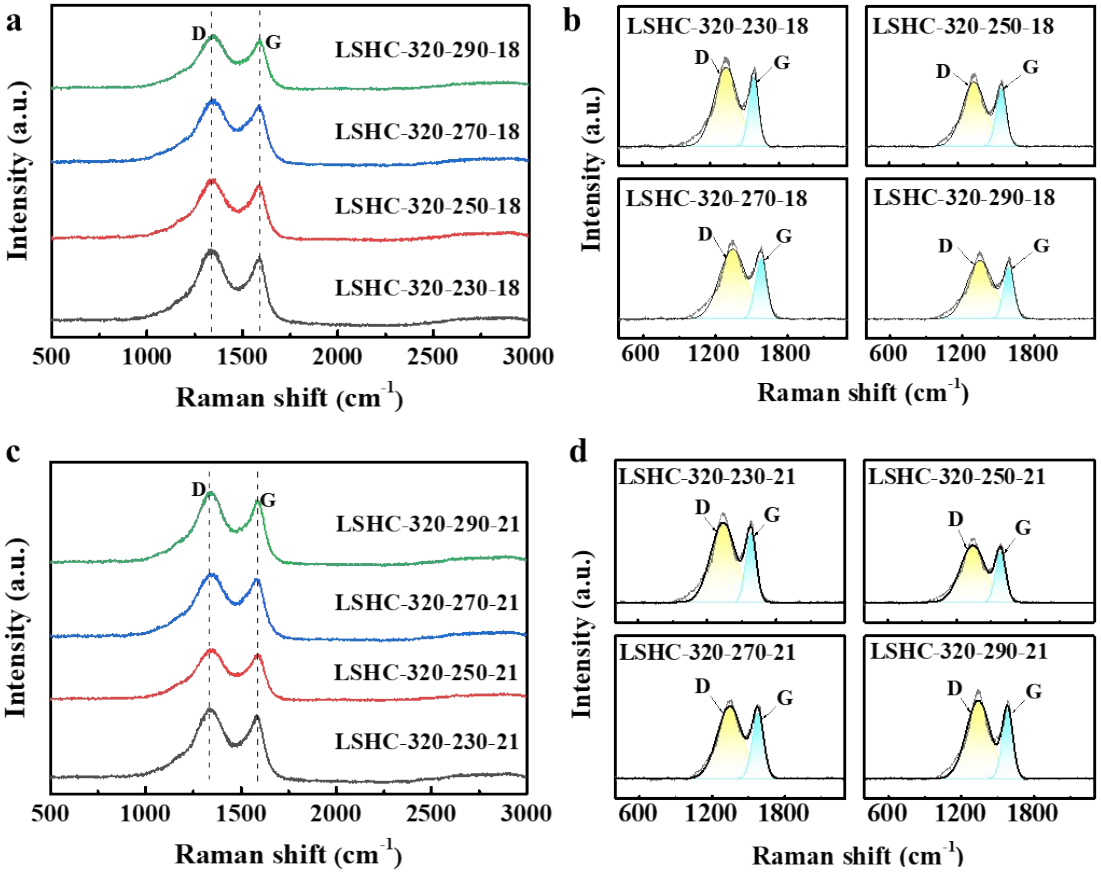

Fig. S8. Raman spectra of lignin samples under different hot-pressing conditions. (a) LSHC-320-230-18, LSHC-320-250-18, LSHC-320-270-18, LSHC-320-290-18 and the corresponding fitting data in (b). (c) LSHC-320-230-21, LSHC-320-250-21, LSHC-320-270-21, LSHC-320-290-21 and the corresponding fitting data in (d).

Table S12. Lattice parameter comparisons of samples under different hot-pressing conditions.

Sample	2θ (002) (°)	d_{002}(nm)	FWHM (002) (°)	L_c (nm)
LSHC-320-230-15	24.50	0.3633	6.75	1.21
LSHC-320-250-15	24.55	0.3626	6.09	1.34
LSHC-320-270-15	24.58	0.3622	5.98	1.36
LSHC-320-290-15	24.59	0.3620	5.86	1.39
LSHC-320-230-18	24.56	0.3625	6.95	1.17
LSHC-320-250-18	24.61	0.3618	6.94	1.17
LSHC-320-270-18	24.67	0.3609	6.87	1.18
LSHC-320-290-18	25.26	0.3525	6.20	1.31
LSHC-320-230-21	24.30	0.3662	6.73	1.21
LSHC-320-250-21	24.31	0.3662	6.55	1.24
LSHC-320-270-21	24.38	0.3650	6.43	1.26
LSHC-320-290-21	25.00	0.3562	5.50	1.48

Table S13. I_D/I_G values of lignin-derived carbon at different hot-pressing conditions.

Sample	I_D/I_G
LSHC-320-230-15	2.67
LSHC-320-250-15	2.17
LSHC-320-270-15	2.51
LSHC-320-290-15	2.57
LSHC-320-230-18	2.80
LSHC-320-250-18	2.70
LSHC-320-270-18	2.57
LSHC-320-290-18	2.42
LSHC-320-230-21	2.80
LSHC-320-250-21	2.78
LSHC-320-270-21	2.60
LSHC-320-290-21	2.51

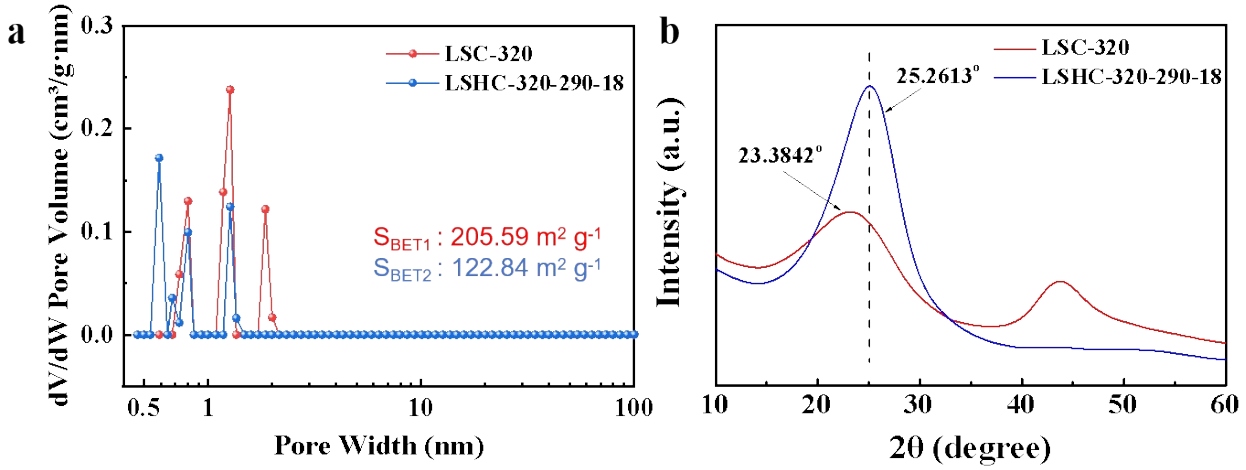

Fig. S9. Comparison between hot-pressing LSHC-320-290-18 and non-hot-pressing LSC-320: (a) Pore size distribution; (b) X-ray diffraction profiles.

LH-Raw-250-15
VS LSH-320-250-

Video S1. The comparison of hot-pressing preparation process of LH-Raw-250-15 and LSH-320-250-15.

References

[S1]Y.-F. Du, G.-H. Sun, Y. Li, J.-Y. Cheng, J.-P. Chen, G. Song, Q.-Q. Kong, L.-J. Xie, C.-M. Chen. Pre-oxidation of lignin precursors for hard carbon anode with boosted lithium-ion storage capacity. Carbon 178 (2021) 243-255, https://doi.org/10.1016/j.carbon.2021.03.016.

[S2]G. Jia, Z. Zhou, Q. Wang, M. T. Innocent, S. Wang, Z. Hu, X. Wang, H. Xiang, M. Zhu. Effect of pre-oxidation temperature and heating rate on the microstructure of lignin carbon fibers. Int. J. Biol. Macromol. 216 (2022) 388-396, https://doi.org/10.1016/j.ijbiomac.2022.06.191.

[S3]Q. Sun, R. Khunsupat, K. Akato, J. Tao, N. Labbé, N. C. Gallego, J. J. Bozell, T. G. Rials, G. A. Tuskan, T. J. Tschaplinski. A study of poplar organosolv lignin after melt rheology treatment as carbon fiber precursors. Green Chem. 18 (18) (2016) 5015-5024, https://doi.org/10.1039/C6GC00977H.

[S4]C. Yang, S. Maldonado, C. R. Stephenson. Electrocatalytic lignin oxidation. ACS Catal. 11 (16) (2021) 10104-10114, https://doi.org/10.1021/acscatal.1c01767.